Volume 22, No 4 | International Journal of Radiation Research, October 2024

A comparison of two low-cost 3D printing techniques for constructing phantoms from MRI breast images

K. Bliznakova[1*], T. Georgiev[1], A. Sarno[2,3], T. Teneva[4], N. Dukov[1], N. Okkalidis[5], Zh. Bliznakov[1]

[1]Department of Medical Equipment, Electronic and Information Technologies in Healthcare, Medical University of Varna, Varna, Bulgaria
[2]Dipartimento di Fisica "Ettore Pancini", Università di Napoli Federico II, Napoli, Italy
[3]INFN Sezione di Napoli, Napoli, Italy
[4]Department of Imaging Diagnostics, Interventional Radiology and Radiotherapy, Medical University of Varna, Bulgaria
[5]Morphé, Thessaloniki, Greece

► ***Original article***

***Corresponding author:**
Dr. Kristina Bliznakova,
E-mail:
kristina.bliznakova@mu-varna.bg

Received: August 2023
Final revised: February 2024
Accepted: April 2024

Int. J. Radiat. Res., October 2024; 22(4): 883-890

DOI: 10.61186/ijrr.22.4.883

Keywords: *3D printing, fused-deposition modeling, inkjet printing, anthropomorphic breast phantoms, X-rays, magnetic resonance images.*

ABSTRACT

Background: This study aimed to test the possibility of using Magnetic Resonance (MR) images to create anthropomorphic breast phantoms for X-ray imaging and to compare the performance of fused deposition modeling (FDM) and 2D inkjet printing with radiopaque inks. ***Materials and Methods:*** Two physical phantoms were produced using either an inkjet printer on paper or an FDM technique, both based on clinical MR data. The paper phantom was printed with 1.2 g of KI dissolved in 20 ml of water. For the FDM phantom, the extrusion rate was adjusted according to clinical Hounsfield unit (HU) values. These phantoms underwent imaging using a clinical computed tomography (CT) device at two energy spectra, and their CT images were assessed in terms of HUs, histogram distributions, spectral and subjective analyses, as well as cost. ***Results:*** The objective CT analysis of the phantoms revealed that HU values and β-values, indicating the anatomical complexity of the breast parenchyma, were in line with those expected, with an advantage for the FDM-based phantom. In both cases, the β-values were close to those for clinical breast images acquired with high-resolution CT scanners. Subjective evaluation, however, indicated a need for refining the realism of the phantoms, particularly in terms of preserving the fine details. ***Conclusion:*** Breast MR Images offer the possibility of constructing breast phantoms. However, the method fails to replicate fine details in phantom CT images. Addressing this challenge requires improvement in segmentation processes and manufacturing accuracy.

INTRODUCTION

Physical breast phantoms are needed for the development of X-ray equipment, for dose assessments, for evaluation of image quality, and for quality assurance programs. Ideally, such phantoms should reflect the physical characteristics of the breast. First, the constituent materials have to present the same X-ray attenuation properties as the breast tissues; and secondly, the phantoms used should reflect the anatomical features of the real organs, such as silhouette, 3D distribution of constituent tissues, and variability (1,2). The required anatomical realism may be derived from clinical images with relatively high spatial resolution acquired with dedicated Breast Computed Tomography (BCT) scanners (2,3). However, this approach is limited by the worldwide scarcity of clinical breast images acquired from BCT scanners (4-6). Conversely, exploiting images acquired by magnetic resonance imaging (MRI) examination has the potential to enrich the available cohort of breast models in terms of both dimensional and anatomical variability. The use of an MRI-based approach to make anthropomorphic breast phantoms has been demonstrated by others to be a valid approach for applications dedicated to microwave imaging diagnosis and biomechanical finite element models (7-9). The creation of physical anthropomorphic breast phantoms for use in X-ray breast imaging investigations needs proper manufacturing technology, suitable materials, and validation of the results, as well as an assessment of time and costs. Various techniques are used for the manufacture of physical breast phantoms, including the mixing of different solid or liquid materials, 3D printing, and 2D inkjet printing (1,2,10). These are steadily improving, in terms of resolution, speed, and suitability of materials, hence allowing the creation of physical anthropomorphic phantoms that ensure radiological equivalence to real human breast tissues.

3D printing technologies have facilitated the design and manufacture of physical breast phantoms, characterized by the realistic representation of internal organ structure. Among the preferred 3D printing techniques are the fused deposition modeling method (FDM) (11-15), stereolithography (SLA) (16,17), polymer jetting (18,19), and inkjet printing (20-23). Of these, the FDM and 2D inkjet printing techniques have been shown to have the lowest cost (1,15, 22,24,25). Both techniques are capable of producing physical models based on either computational breast models or patient images from medical scans or mammography examinations. This study was designed to evaluate the phantoms generated from MRI images, and was intended both to test the feasibility of this approach and to compare the two manufacturing methods. The novelty of the paper lies in the use of magnetic resonance (MR) breast images, which are more widely accessible than images acquired via BCT scanners and are of relatively high resolution (2). The goal was to explore the possibility of creating an extensive collection of phantoms that accurately represent the large variability in breast anatomy. Additionally, we aimed to assess the potential of inkjet-printed breast phantoms in 3D imaging, an area that, until now, has been primarily confined to 2D imaging. For this purpose, phantoms based on the same digital breast model were produced both by FDM and 2D inkjet methods. The assessment consisted of measurement of the CT numbers (in Hounsfield Unit, HU) from CT images of the manufactured phantoms, and evaluation of both histogram distributions and replicated anatomical noise background. In addition, subjective analysis was carried out by an experienced radiologist.

MATERIALS AND METHODS

The physical breast phantoms, named Paper phantom and FDM phantom, were developed using the patient's MR segmented images, available in an open-access database published on Zenodo.org (26). The FDM phantom was fabricated based on a 3D printing technology that associates HU with a corresponding filament extrusion rate in order to tune the local density of the printed material (25), while the Paper phantom was fabricated using 2D inkjet technology based on the association of the CT number with the ink-iodine mixture quantity (that is, greyscale values). The manufactured physical phantoms were imaged in a clinical CT scanner and evaluated in terms of reproduced CT numbers and anatomical noise. The study overview is shown in figure 1.

Phantoms

Patient data and computational phantoms

The MR images used for the creation of the anthropomorphic phantoms were acquired with a GE Signa HDxt MRI scanner (GE Healthcare, USA) employing a T1-weighted Axial multi-phase VIBRANT (3-phase) sequence, incorporating contrast-enhanced administration and fat suppression (figure 2). The voxel size was 0.7 mm × 0.7 mm × 0.8 mm (25). The original patient data were segmented into adipose, glandular, skin, and tumor tissues, each assigned a specific HU value in the resulting segmented digital breast phantom: -152 (adipose), 42 (glandular tissue) and 108 (skin) and 64 (tumor).

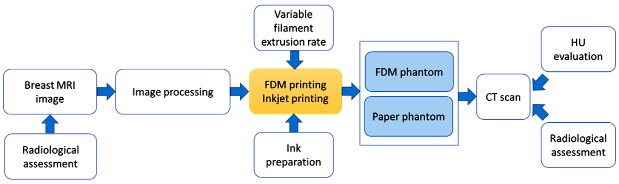

Figure 1. A diagram of the experimental investigation. FDM and Paper phantoms were both created from patient MR images. The original patient data were segmented into the different breast tissues, to which specific HU values were assigned. Phantoms were then printed by 2D inkjet and FDM techniques, and scanned at a clinical CT unit. The results were evaluated quantitatively and qualitatively.

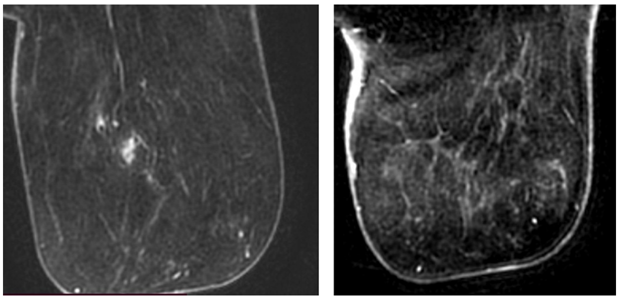

Figure 2. Two MR images with observed skin, neoplastic, glandular, and adipose tissues. These images are part of the dataset used for the creation of the computational model (26) that was utilized for the physical FDM and Paper phantoms.

FDM-based phantoms

The FDM phantom, shown in figure 3a, was developed in our previous studies (25). A crucial step in its development was the calibration procedure, necessary to establish the correct extrusion speed to achieve the desired HUs in the final images. For this purpose, we printed several groups of cubes, with dimensions 20 mm × 20 mm × 20 mm, using different filament extrusion rates. The cubes were imaged at a clinical CT unit and the retrieved HU were correlated with the filament extrusion rates.

The FDM phantom was fabricated by extruding a constant amount of filament per voxel and employing a perimetric pattern to replicate irregularly shaped entities, corresponding to glandular and tumor tissues. Glandular, adipose, and skin tissues were printed using three constant filament extrusion rates correlated with three HU values derived from the calibration processes. The FDM phantom was made with an FDM printer MT2-B (Multoo, China), which has printing dimensions 500mm×500mm×600mm

[DOI: 10.61186/ijrr.22.4.883]

and PLA filament from Formfutura (Holland) with a density of 1.24 g cm^{-3} and 1.75 mm diameter. The thickness of the printed layer was 0.25 mm and therefore each MR image was replicated by printing three identical layers.

Paper-based phantoms

The inkjet printing method uses an inkjet printer with a specially prepared iodine-based ink, which can be "seen" in a CT scanner. Each slice from the segmented MRI volume was binarized; the voxels that corresponded to adipose tissue were set to 255, and the glandular and skin values were transformed to 0. The iodine-based ink mixture consisted of 1.2 g KI dissolved in 20 ml of water. To this mixture, 1 ml of standard ink was added in order to visualize the printed structures on the paper, since the KI solution is transparent. The mixture was injected into the empty printer cartridge of an HP Officejet 5510 printer. The amount of ink was calculated by using the NIST database (27) and the relationship between CT numbers and X-ray attenuation coefficients (28).

The printed Paper phantom was based on 30 consecutive slices from the segmented image set, and each slice in printed form was on eight sheets of plain A4 office paper: thus the printed phantom consisted of a total of 240 sheets with a thickness of 24 mm. The skin and glandular tissues were printed with 100% ink infill. The phantom that was produced is shown in figure 3b. Polymethyl methacrylate (PMMA) sheets, each with a thickness of 5 mm, were used as the upper and lower surfaces to secure the phantom and eliminate air.

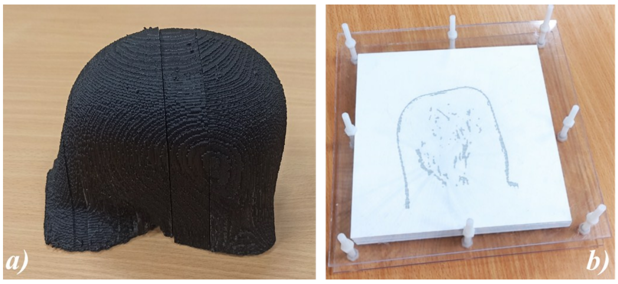

Figure 3. Phantoms used in the study: **(a)** FDM phantom, **(b)** Paper phantom. The digital source of these phantoms was the same.

Experimental work and evaluation

CT images of the phantoms were acquired at the "St. Marina" University Hospital of Varna (Bulgaria) using a Siemens Somatom Force CT scanner (Siemens, Germany) and an abdomen standard protocol at 70 kV and 120 kV. The 70 kV was the lowest possible X-ray energy and was within the range of the tube voltages used in a dedicated breast CT scanner (29). The reconstructed slice thickness was 0.5 mm, the convolution Kernel was Br40d and the coronal pixel size was 0.45 mm × 0.45 mm. Images were first examined visually, followed by an objective evaluation using ImageJ (https://imagej.nih.gov/ij/).

Subjective evaluation comprised visual observation of the images and a comparison of the contrast and shape of the tissue-mimicking structures in the images. Objective evaluation included comparison of CT numbers from slices of clinical 3D breast images, literature data, and calculation of histogram distributions and of the β parameter as an indication of the anatomical noise (30). For evaluation of the CT numbers, regions of interest of size 20 pixels ×20 pixels were defined automatically with the radiomics platform of Marinov *et al* (31). An example of one of the slices is shown in figure 4.

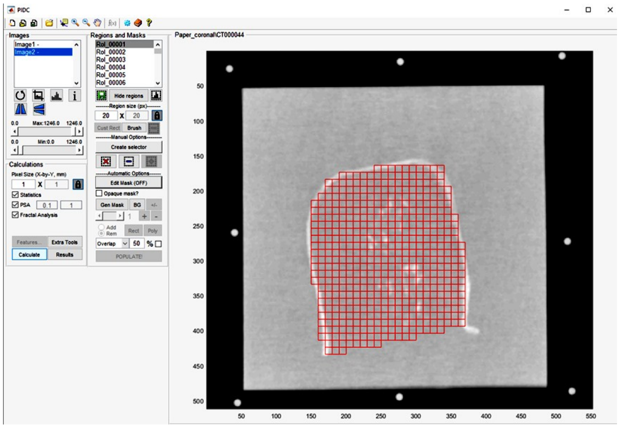

Region size (px): 20 x 20

Pixel Size (X-by-Y, mm): 1 x 1

☑ Statistics

☑ PSA 0.1 1

☑ Fractal Analysis

☐ Opaque mask?

Overlap 50 % ☐

Max:1246.0 1246.0

Min:0.0 1246.0

Figure 4. Defining the HU histogram and other features by means of a radiomics software program (31).

For spectral analysis, the β parameter, which quantitatively describes the anatomical complexity or anatomical noise of the texture related to the healthy tissues in the breast images (30,32), was evaluated. This parameter was used to evaluate how appropriately the phantoms mimicked the tissue background in organ images. The β parameter usually presents values close to 3 in breast images acquired via digital mammography and breast tomosynthesis, reducing to 2 for CT images, in which the anatomical noise is less pronounced (30,32,33). In order to evaluate β for CT images of the manufactured breast phantoms, the average 2D NPS (Noise Power Spectrum) was evaluated in 1000 ROIs (Regions of Interest), each comprising 128 × 128 pixels. Various ROIs were randomly selected in the CT images of the scanned physical phantoms with a reconstructed pixel pitch of 0.912 mm and processed as suggested by Chen *et al.* (30). The 1D Noise Power Spectrum (NPS) was computed as the radial profile of the 2D NPS curve. The β parameter was evaluated as the absolute value of the linear fit curve slope of the 1D NPS curve in an appropriate frequency range comprised between 0.04 mm^{-1} and 0.40 mm^{-1}. This range was tuned in order to maximize linear model suitability.

RESULTS

Printed physical phantoms and CT images

CT images of the two physical phantoms, scanned

[DOI: 10.61186/ijrr.22.4.883]

in the clinical CT scanner, are shown in figure 5.

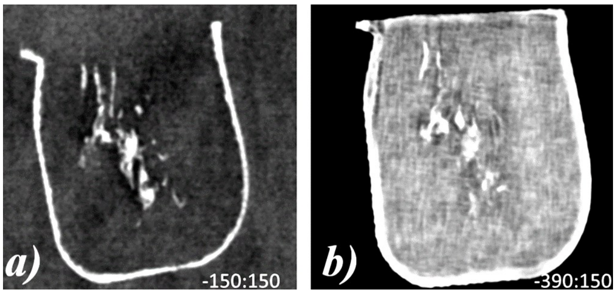

Figure 5. Selected slices from the CT scans of: (a) Paper phantom and (b) FDM phantom. The windowing display settings are marked on the corresponding images, acquired at 70 kV.

Figure 6 depicts the histogram distributions of the selected CT scans for the Paper phantom (figures 6a and 6b) and the FDM phantom (figures 6c and 6d) at 70 kV (figures 6a and 6c) and 120 kV (figures 6b and 6d). The largest peaks correspond to the adipose tissue. Average HU values obtained from selected ROIs in the CT images are reported in table 1. In this table, measured CT numbers from literature are also reported, derived both from CT images of equivalent materials and from breast tissues. Specifically, the HU values assessed at 70 kV (with an average energy of 41 keV) for the FDM phantom closely aligned with the CT numbers documented by Geeraert (34) for tissue-equivalent materials evaluated within the range of 40 – 54 keV for corresponding tissues. This agreement was weaker for the Paper phantom, for which HU values were lower for both adipose and glandular tissues. This may have been due to the presence of trapped air between the paper sheets. While this presents minimal impact on 2D projection images (20,22), in 3D images of the Paper phantom, external pressure applied to the stacked sheets could alter the air content and subsequently influence the final HU values. A dedicated study is needed to evaluate this aspect.

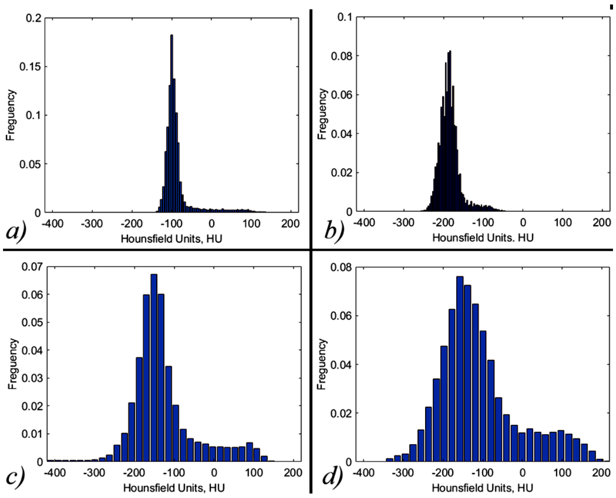

Figure 6. Normalized histogram distributions of a selected slice from a-b) Paper phantom and c-d) FDM phantom. The physical phantoms were scanned at 70 kV **(a-c)** and 120 kV **(b-d)**. Bin counts were set to 64.

Table 1. Comparison of measured HUs with data from the literature.

		Glandular, average HU	Adipose, average HU
70 kV	Paper phantom	39 ± 4	-88 ± 11
	FDM phantom	57 ± 19	-129 ± 10
120 kV	Paper phantom	-78 ± 6	-188 ± 12
	FDM phantom	45 ± 19	-131 ± 15
40 keV*		57	-144
54 keV*		42	-111
80 kV**		44	-138
120 kV***		40	-100

*data taken from ref (34), **data taken from ref (25), ***data taken from ref (35).

Evaluation of β parameter

Figure 7 shows the 1D NPS curves from the phantom images shown in figure 5. They are represented on a log-log scale and the linear fit is shown in red.

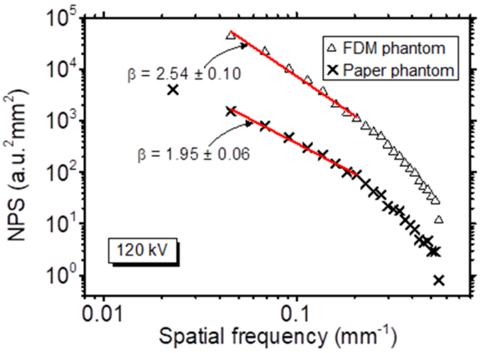

Figure 7. Noise Power Spectrum (NPS) on a log-log scale evaluated over the anatomical background from 3D images represented in figure 5. Red lines represent the linear fit curves whose slopes furnish the β values. Data are shown for 120kV. Since the β value describes the anatomical complexity of the organ in the acquired image, it shows negligible dependence on the beam energy (33).

The β parameter was evaluated as 2.54 ± 0.10 for the FDM- based phantom and 1.95 ± 0.06 for the paper-based phantom. For 3D images of the breast, it is expected to have a value close to 2.

Radiological assessment and printing and cost-effective parameters

An assessment of the phantom images that were obtained was performed subjectively by an experienced radiologist certified in general radiology and with more than 3 years of experience in breast imaging. In the original breast MR image, the radiologist was able to distinguish the following anatomical structures: 1) connective tissue consisting of mammary glands and ducts, small vessels, lymph vessels, and nerves, 2) adipose tissue consisting of fatty structures, 3) greater vessels (arteries and/or veins) in the periphery of the breast and 4) skin (again soft tissue component). Normal connective tissue was more visible, and was therefore considered to be more significant than glands. Pathological structures, including the neoplasm, were seen, but were not taken into account for the phantom

[DOI: 10.61186/ijrr.22.4.883]

manufacturing process and they are included inside the phantom as part of the fibroglandular tissue, since they show the same density.

Connective tissue, vessels, and skin showed as hyperintense or brighter in MR images, while adipose tissue exhibits hypointensity or appears darker due to distinct attenuation patterns (figure 2). Conversely, in CT images, connective tissue, vessels, and skin display hyperdensity or brightness, while adipose tissue assumes hypodensity or appears darker. When comparing the MR image and the CT phantom image, a very good overlap between the two imaging techniques was observed, with minimal loss of information (in the CT image) about subtle details. The disparity was negligible for the chosen breast model (ACR breast composition A, featuring a readily visible tumor). However, it may present challenges in other scenarios not addressed in this paper (e.g., ACR breast composition C, with a non-visible tumor).

The original breast composition is primarily composed of fatty tissue; thus, interpreting MR and CT images posed fewer challenges. In this setting the contrast of the internal breast structures was enhanced and the interpretation was more comprehensive. The four criteria used by the radiologist to assess both MR and CT images were: description of the anatomical structures; tissue contrast; comparison between original MR images and CT images of the physical phantoms and radiological realism of the phantoms. The evaluation is summarized as follows: (1) Anatomical structures: Based on the anatomy of the normal breast and the individual anatomical features of the scanned breast, three breast tissues are distinguishable – adipose and glandular tissues, and skin. While fine details may not be distinct, the differentiation between glandular and adipose tissue is evident due to heightened image contrast; (2) Tissue contrast: The image contrast is very good for each image as well as between the different slices. The distinction between glandular and adipose tissues, although not capturing fine details, is discernible due to pronounced image contrast; (3) Image comparison: Despite the different scanning techniques employed, MR and phantom images exhibit strong correspondence (in terms of represented tissues); (4) Radiological realism: achieving a total realistic representation remains elusive. Improved training for segmentation and interpretation processes will require additional clinical and imaging data.

A comparison of CT images of Paper and FDM breast phantoms is summarized in table 2 regarding the four criteria mentioned above. The radiologist's final report concluded in favor of the FDM phantom, with an overall better image quality and enhanced tissue contrast.

Printing time, cost, and assessment of the phantom realism are summarized in table 2. The printing time indicates only the printing hours and does not include the time needed for image processing, ink preparation, and 3D printer adjustments. The costs for the printed phantoms include only the used materials. Costs do not include the operator's time costs, nor the initial investments for the printers.

Table 2. Comparison of CT images of Paper and FDM breast phantoms with respect to anatomical structures, tissue contrast, image comparison, and realistic representation of the models. The manufacturing time and cost of the phantoms are summarized in the last two columns.

Phantom	Anatomy	Tissue contrast	Image comparison	Realism	Time for printing, hours	Cost, EUR
Paper	Only glands and skin, no fine details	Sharp tissue contrast	Not satisfying enough	A realistic representation of the CT-scanned phantom in comparison to an MRI is not achievable.	4(30*)	2(10*)
FDM	All- glands, adipose, skin, no fine details	Tissue contrast as sharp as the CT slice	Stronger correspondence	A realistic representation of the CT scanned phantom in comparison to MRI is achievable, but still missing small details. Overall the CT image is of better quality.	120	30

*Calculated data for the whole breast volume.

DISCUSSION

Lately, both fused deposition modeling and inkjet printing with radiopaque inks have been intensively used for the creation of physical phantoms for testing X-ray equipment. Specifically, in the field of X-ray breast imaging, anthropomorphic physical breast phantoms find applications for quality control of radiological systems, as well as for testing and optimization of advanced breast imaging techniques (1,10). The limited availability of high-resolution 3D breast images acquired via dedicated CT scanners led us to investigate the possibility of using MR breast images for model preparation.

Until now, inkjet-printed phantoms have primarily been used for assessing image quality in 2D digital mammography and digital breast tomosynthesis (18,20,22,36,37). In this study, for the first time, we investigated the possibility of extending such a technique to the 3D case by employing a 2D inkjet printer with an office plain paper sheet. This is an advantage compared to the use of the more expensive iohexol and the relatively thicker parchment paper (38). A visual comparison of the selected CT slices from the scanned physical phantoms shows that both phantoms provided a contrast between the adipose and glandular tissues.

HU histograms of CT images of the manufactured

[DOI: 10.61186/ijrr.22.4.883]

phantoms reveal that both techniques, the FDM with tunable extrude speed and the inkjet printer with office paper, can reproduce adipose, glandular, and skin values, as the areas corresponding to these structures are visible. Among the two phantoms compared, the FDM phantom demonstrates a highly comparable HU distribution and trend to the corresponding adipose and glandular tissues (34,39). A disadvantage of the FDM printing process is the longer time needed for manufacturing the anthropomorphic breast phantom and the necessity to restart from the beginning of the complete printing process if there is an error while printing. Another limitation is the need for a calibration phantom and calibration procedure, and this should be applied for each energy. The radiologists noted the visible pattern, which may eventually be removed by changing the method for FDM printing (40, 41) or by applying filtering in the frequency domain.

In the case of the Paper phantom, an increase in the kV resulted in a shift of the HU histogram towards lower CT numbers. This phenomenon can be attributed to the composition of office paper, which includes calcium, as reported by Gong *et al.* (42). Moreover, the ink component of the paper contains iodine, leading to an increased occurrence of photoelectric events and subsequently enhanced attenuation (43). This outcome suggests that phantoms based on office paper, such as the one studied, may not be suitable for comprehensive utilization across all ranges of kV. Further, some challenges were present during the inkjet printing process, such as the need to continuously supervise the whole process in order to prevent paper jams, ink drying, or possible clogging, and to replace or refill ink cartridges regularly. Clogging, streaks, the need for a flush, and several printer head failures during an inkjet print have also been reported by other researchers (44). Another challenge was the paper outside the printed breast structures. This paper must be cut after the whole physical phantom is assembled as close as possible to the external breast contour. Alignment of paper sheets is also crucial.

The power spectrum analysis of the phantom images suggests that the anatomical noise of the images of the paper-based and the FDM-based generated phantoms reflects that of clinical 3D breast images with a β value of about 2 (30,32). Hence, this parameter was shown to quantify the noise background in the X-ray breast images, reducing from a value of 3, evaluated in digital mammography and digital breast tomosynthesis, down to 2 in BCT, where the tissue superimposition and the related anatomical noise are reduced. The evaluation of the β parameter was intended to test the degree of reproduction of the anatomical background noise in the developed phantoms. Limitations of this evaluation are related to the use of a whole-body CT scanner that produces images whose slice thickness is almost twice that used in the BCT studies (30,32). This may yield slightly larger β values than the expected value of 2. The Paper phantom presented the lowest β value (1.95 ± 0.06), in line with the expected values. It was slightly higher for the FDM case (2.54 ± 0.10).

A comparison of the two printing techniques showed that 2D inkjet printing is approximately three times cheaper than FDM printing, taking into account only the costs of the used consumables. Additionally, several studies revealed that the initial investment in printing equipment is cheaper for inkjet printing (20). In this study, for implementing the 2D inkjet printing, we used a general-purpose desktop inkjet printer, which costs about 50 euros. For FDM printing, the cheapest FDM commercially available printers for hobbyists that are suitable for this purpose cost about 200 euros. The improvement of 3D printing technologies allows for sufficient printing accuracy and thus satisfactory completion of the printed object. These types of printers allow both commercial upgrades and custom development of hardware and in-house software codes. This strong advantage, together with the good quality of images produced with FDM printers, showed that this technique could be successfully used for the manufacture of anthropomorphic phantoms for quality control, as well as for personalized diagnostic imaging.

The involved radiologist reviewed the CT images of both phantoms and affirmed that “Realistic representation of the CT scanned phantom in comparison to MRI is achievable, still missing small details”. This shortcoming may be alleviated by improvement of the segmentation algorithm as well as by reaching smaller spatial resolutions in the manufacturing processes.

Future work will be focused on the improvement of current and production of new printing materials suitable for use with these two technologies. The comparison of KI and PLA as basic materials for printing models for X-ray imaging shows that using a 100% PLA is not appropriate for use with X-rays in the diagnostic energy range. KI is suitable for diagnostic X-ray imaging in certain concentrations (20-22). The concentration of KI is easy to change, while PLA with varying densities can be produced only with dedicated software, not commercially available (13,45). The software for paper printing is freely available, while the non-commercially dedicated software for FDM printers needs proper licensing. Newly manufactured materials, however, need to be carefully assessed for their suitability for use with the specific printing technologies and they have to be evaluated for their radiological properties. Therefore, the interdisciplinary team involved in this work is currently focusing on evaluating new materials, developed by our mechanical engineer, which will further be scanned at a micro CT facility and chemically analyzed in order to propose better printing materials and a better methodology for

[DOI: 10.61186/ijrr.22.4.883]

printing anthropomorphic breast phantoms.

CONCLUSION

This study evaluated the possibility of exploiting MR breast images for the manufacture of uncompressed breast phantoms by using two low-cost printing technologies. HU values and β-values – indicating the anatomical complexity of the breast parenchyma – are in line with those expected, with an advantage for the FDM phantom. However, a subjective analysis conducted by an experienced radiologist outlined a continued deficiency in the realism of CT images of the phantoms when compared to MR breast original images, with a loss of fine details during the processes.

AKNOWLEDGMENT

This study received funding from the European Union's Horizon 2020 Research and Innovation Program under the Marie Skłodowska-Curie grant agreement No 101008020. The PHENOMENO team is grateful to Professor Ilyan Kolev from the Medical University of Varna for providing KI for the Paper phantom.

Ethical issues: This study was approved by the Ethics Committee of the Medical University of Varna (Approval number 102/22.04.2021).

Conflict of interest: There is no conflict of interest.

Authorship: Authors of this publication have made the following contributions: K.B. - the concept, methodology, scanning the phantoms, evaluation of results, writing the original draft; T.G. - producing the ink-based model, measuring the HU of gland and adipose, data from the literature, writing the original draft; A.S. - calculation of the beta parameter from CT phantom images, revising the draft; T.T. - radiologist of the study, evaluating all images, description of the radiological assessment and revising the draft; N.D. - segmenting the MR image, scanning the phantoms, revising the draft; N.O. - producing the FDM phantom, revising the draft; Z.B. – scanning the phantoms, revising the draft.

REFERENCES

1. Bliznakova K (2020) The advent of anthropomorphic three-dimensional breast phantoms for X-ray imaging. *Phys Med*, ***79:*** *145-161. DOI: 10.1016/j.ejmp.2020.11.025.*
2. Sarno A, Valero C, Tucciariello RM, Dukov N, Costa PR, Tomal A (2023) Physical and digital phantoms for 2D and 3D x-ray breast imaging: Review on the state-of-the-art and future prospects. *Radiat Phys Chem*, ***204:*** *110715. DOI: https://doi.org/10.1016/j.radphyschem.2022.110715.*
3. Sarno A, Mettivier G, di Franco F, Varallo A, Bliznakova K, Hernandez AM and Russo P (2021) Dataset of patient-derived digital breast phantoms for in silico studies in breast computed tomography, digital breast tomosynthesis, and digital mammography. *Med Phys*, ***48:*** *2682-2693. DOI: 10.1002/mp.14826.*
4. Schmidt CS, Zellweger C, Wieler J, Berger N, Marcon M, Frauenfelder T and Boss A (2022) Clinical assessment of image quality, usability and patient comfort in dedicated spiral breast computed tomography. *Clin Imaging*, ***90:*** *50-58. DOI: 10.1016/j.clinimag.2022.07.001.*
5. Zhu Y, O'Connell AM, Ma Y, Liu A, Li H, Zhang Y, *et al*. (2022) Dedicated breast CT: state of the art-Part I. Historical evolution and technical aspects. *Eur Radiol*, ***32:*** *1579-1589. DOI: 10.1007/s00330-021-08179-z.*
6. Zhu Y, O'Connell AM, Ma Y, Liu A, Li H, Zhang Y, *et al*. (2022) Dedicated breast CT: state of the art-Part II. Clinical application and future outlook. *Eur Radiol*, ***32:*** *2286-2300. DOI: 10.1007/s00330-021-08178-0.*
7. Pelicano AC, Goncalves MCT, Godinho DM, Castela T, Orvalho ML, Araujo NAM, *et al*. (2021) Development of 3D MRI-Based Anatomically Realistic Models of Breast Tissues and Tumours for Microwave Imaging Diagnosis. *Sensors*, ***21:*** *8265. DOI: 10.3390/s21248265.*
8. Godinho DM, Felicio JM, Castela T, Silva NA, Orvalho ML, Fernandes CA, *et al*. (2021) Development of MRI-based axillary numerical models and estimation of axillary lymph node dielectric properties for microwave imaging. *Med Phys*, ***48:*** *5974-90. DOI: 10.1002/mp.15143.*
9. Garcia E, Diez Y, Diaz O, Llado X, Marti R, Marti J, *et al*. (2018) A step-by-step review on patient-specific biomechanical finite element models for breast MRI to x-ray mammography registration. *Med Phys*, ***45:*** *e6-e31 DOI: 10.1002/mp.12673.*
10. Glick SJ, Ikejimba LC (2018) Advances in digital and physical anthropomorphic breast phantoms for x-ray imaging. *Med Phys*, ***45:*** *e870-e85. DOI: 10.1002/mp.13110.*
11. di Franco F, Sarno A, Mettivier G, Hernandez AM, Bliznakova K, Boone JM, *et al*. (2020) GEANT4 Monte Carlo simulations for virtual clinical trials in breast X-ray imaging: Proof of concept. *Phys Med*, ***74:*** *133-142. DOI: S1120-1797(20)30123-X [10.1016/j.ejmp.2020.05.007].*
12. Dukov NT, Feradov FN, Gospodinova GD, Bliznakova KS (2019) An approach for printing tissue-mimicking abnormalities dedicated to applications in breast imaging. 28th International Scientific Conference Electronics, ET 2019 - Proceedings: Institute of Electrical and Electronics Engineers Inc.; DOI: 10.1109/et.2019.8878587.
13. Mei K, Geagan M, Roshkovan L, Litt HI, Gang GJ, Shapira N, *et al*. (2022) Three-dimensional printing of patient-specific lung phantoms for CT imaging: Emulating lung tissue with accurate attenuation profiles and textures. *Med Phys*, ***49:*** *825-835. DOI: 10.1002/mp.15407.*
14. Varallo A, Sarno A, Castriconi R, Mazzilli A, Loria A, Del Vecchio A, *et al*. (2022) Fabrication of 3D printed patient-derived anthropomorphic breast phantoms for mammography and digital breast tomosynthesis: Imaging assessment with clinical X-ray spectra. *Phys Med*, ***98:*** *88-97. DOI: https://doi.org/10.1016/j.ejmp.2022.04.006.*
15. Mettivier G, Sarno A, di Franco F, Bliznakova K, Bliznakov Z, Hernandez AM, *et al*. (2019) The Napoli-Varna-Davis project for virtual clinical trials in X-ray breast imaging. IEEE Nuclear Science Symposium and Medical Imaging Conference (NSS/MIC), Manchester, UK, pp. 1-5, DOI: 10.1109/NSS/MIC42101.2019.9059828.
16. Carton AK, Bakic P, Ullberg C, Derand H, Maidment AD (2011) Development of a physical 3D anthropomorphic breast phantom. *Med Phys*, ***38:*** *891-896. DOI: 10.1118/1.3533896.*
17. Kiarashi N, Nolte AC, Sturgeon GM, Segars WP, Ghate SV, Nolte LW, *et al*. (2015) Development of realistic physical breast phantoms matched to virtual breast phantoms based on human subject data. *Med Phys*, ***42:*** *4116-4126. DOI: 10.1118/1.4919771.*
18. Badal A, Clark M, Ghammraoui B (2018) Reproducing two-dimensional mammograms with three-dimensional printed phantoms. *J Med Imaging,* ***5:*** *033501 DOI: 10.1117/1.JMI.5.3.033501 17353PRR.*
19. Schopphoven S, Cavael P, Bock K, Fiebich M, Mader U (2019) Breast phantoms for 2D digital mammography with realistic anatomical structures and attenuation characteristics based on clinical images using 3D printing. *Phys Med Biol*, ***64:*** *215005. DOI: 10.1088/1361-6560/ab3f6a.*
20. Ikejimba LC, Graff CG, Rosenthal S, Badal A, Ghammraoui B, Lo JY, *et al*. (2017) A novel physical anthropomorphic breast phantom for 2D and 3D x-ray imaging. *Med Phys*, ***44:*** *407-416. DOI: 10.1002/mp.12062.*
21. Georgiev T, Kolev I, Dukov N, Mavrodinova S, Yordanova M, Bliznakova K (2021) Development of an inkjet calibration phantom for X-

ray imaging studies. *Scripta Scientifica Medica*, ***53:*** *15-20 DOI: http://dx.doi.org/10.14748/ssm.v0i0.7410.*

22. Ikejimba LC, Salad J, Graff CG, Goodsitt M, Chan HP, Huang H, *et al*. (2021) Assessment of task-based performance from five clinical DBT systems using an anthropomorphic breast phantom. *Med Phys*, ***48:*** *1026-1038. DOI: 10.1002/mp.14568.*
23. Jahnke P, Limberg FRP, Gerbl A, Pardo GLA, Braun VPB, Hamm B, *et al*. (2017) Radiopaque three-dimensional printing: A method to create realistic CT phantoms. *Radiology*, ***282:*** *569-575. DOI: 10.1148/radiol.2016152710.*
24. Ivanov D, Bliznakova K, Buliev I, Popov P, Mettivier G, Russo P, *et al*. (2018) Suitability of low density materials for 3D printing of physical breast phantoms. *Phys Med Biol*, ***63:*** *175020. DOI: 10.1088/1361-6560/aad315.*
25. Dukov N, Bliznakova K, Okkalidis N, Teneva T, Encheva E, Bliznakov Z (2022) Thermoplastic 3D printing technology using a single filament for producing realistic patient-derived breast models. *Phys Med Biol*, ***67:*** *045008, DOI: 10.1088/1361-6560/ac4c30.*
26. Dukov N, Bliznakova K, Okkalidis N, Teneva T, Encheva E, Bliznakov Z (2021) Patient breast MRI images and computational breast phantom data for research in patient-derived realistic breast modelling (Versione 1) [Data set]. Zenodo. https://doi.org/10.5281/zenodo.5887359
27. Berger MJ, Hubbell JH, Seltzer SM, Chang J, Coursey JS, Sukumar R, Zucker DS and Olsen K (2010) XCOM: Photon Cross Section Database (version 1.5). [Online] Available: http://physics.nist.gov/xcom [2023, August 23]. National Institute of Standards and Technology, Gaithersburg, MD.
28. Bryant JA, Drage NA, Richmond S (2012) CT number definition. *Radiat Phys Chem*, ***81:*** *358-361. DOI: 10.1016/j.radphyschem.2011.12.026.*
29. Metheany KG, Abbey CK, Packard N, Boone JM (2008) Characterizing anatomical variability in breast CT images. *Med Phys*, ***35:*** *4685-4694. DOI: 10.1118/1.2977772.*
30. Chen L, Abbey CK, Nosrateih A, Lindfors KK, Boone JM (2012) Anatomical complexity in breast parenchyma and its implications for optimal breast imaging strategies. *Med Phys,* ***39:*** *1435-1441. DOI: 10.1118/1.3685462.*
31. Marinov S, Buliev I, Cockmartin L, Bosmans H, Bliznakov Z, Mettivier G, *et al*. (2021) Radiomics software for breast imaging optimization and simulation studies. *Phys Med,* ***89:*** *114-128. DOI: https://doi.org/10.1016/j.ejmp.2021.07.014.*
32. Chen L, Abbey CK, Boone JM (2013)Association between power law coefficients of the anatomical noise power spectrum and lesion detectability in breast imaging modalities. *Phys Med Biol,* ***58:*** *1663-1681. DOI: 10.1088/0031-9155/58/6/1663.*
33. Mettivier G, Bliznakova K, Sechopoulos I, Boone JM, Di Lillo F, Sarno A, *et al*. (2017) Evaluation of the BreastSimulator software platform for breast tomography. *Phys Med Biol*, ***62:*** *6446-6466 DOI: 10.1088/1361-6560/aa6ca3.*
34. Geeraert N (2014) "Quantitative evaluation of fibroglandular tissue for estimation of tissue-differentiated absorbed energy in breast tomosynthesis" Doctorat ParisTech Thesis.
35. Ruschin M, Davidson SRH, Phounsy W, Yoo TS, Chin L, Pignol JP, *et al*. (2016) Technical Note: Multipurpose CT, ultrasound, and MRI breast phantom for use in radiotherapy and minimally invasive interventions. *Med Phys*, ***43:*** *2508-2514. DOI: 10.1118/1.4947124.*
36. Zhao C, Solomon J, Sturgeon GM, Gehm ME, Catenacci M, Wiley BJ and Lo JY (2017) Third generation anthropomorphic physical phantom for mammography and DBT: incorporating voxelized 3D printing and uniform chest wall QC region. *In Medical Imaging Physics of Medical Imaging*, ***10132:*** *479-486. DOI: 10.1117/12.2256091.*
37. Clark M, Ghammraoui B and Badal A (2016) Reproducing 2D breast mammography images with 3D printed phantoms. *Medical Imaging Physics of Medical Imaging*, ***9783:*** *89-97. DOI: 10.1117/12.2217215.*
38. Ikejimba LC, Salad J, Graff CG, Ghammraoui B, Cheng WC, Lo JY, *et al*. (2019) A four-alternative forced choice (4AFC) methodology for evaluating microcalcification detection in clinical full-field digital mammography (FFDM) and digital breast tomosynthesis (DBT) systems using an inkjet-printed anthropomorphic phantom. *Med Phys*, ***46:*** *3883-3892. DOI: 10.1002/mp.13629.*
39. Ma X, Figl M, Unger E, Buschmann M, Homolka P (2022) X-ray attenuation of bone, soft and adipose tissue in CT from 70 to 140 kV and comparison with 3D printable additive manufacturing materials. *Sci Rep*, ***12:*** *14580. 10.1038/s41598-022-18741-4.*
40. Mettivier G, Sarno A, Varallo A, Russo P (2022) Attenuation coefficient in the energy range 14-36 keV of 3D printing materials for physical breast phantoms. *Phys Med Biol*, ***67:*** *Artn 175012, DOI: 10.1088/1361-6560/Ac8966.*
41. Okkalidis N, Bliznakova K, Kolev N (2022) A filament 3D printing approach for CT-compatible bone tissues replication. *Phys Med*, ***102:*** *96-102. DOI: 10.1016/j.ejmp.2022.09.009.*
42. Gong Z, Shen H, Yang X, *et al*. (2014) Lipid production from corn stover by the oleaginous yeast Cryptococcus curvatus. *Biotechnol Biofuels,* ***23:*** *158. DOI: 10.1186/s13068-014-0158-y.*
43. Kozee M, Weygand J, Andreozzi JM, Hunt D, Perez BA, Graham JA, Redler G (2023) Methodology for computed tomography characterization of commercially available 3D printing materials for use in radiology/radiation oncology. *J Appl Clin Med Phys*, ***24****: e139993. DOI: 10.1002/acm2.13999.*
44. Pegues H, Knudsen J, Tong HY, Gehm ME, Wiley BJ, Samei E, *et al*. (2019) Using inkjet 3D printing to create contrast-enhanced textured physical phantoms for CT. Medical Imaging: Physics of Medical Imaging, Artn 109484z. DOI: 10.1117/12.2512890.
45. Okkalidis N (2018) A novel 3D printing method for accurate anatomy replication in patient-specific phantoms. *Med Phys*, ***45:*** *4600-4606. DOI: 10.1002/mp.13154.*

[DOI: 10.61186/ijrr.22.4.883]